International Journal of Nanomedicine

Dovepress

open access to scientific and medical research

Open Access Full Text Article

ORIGINAL RESEARCH

Noninvasive Photothermal Therapy of Nasopharyngeal Cancer Guided by High Efficiency Optical-Absorption Nanomaterial Enhanced by NIR-II Photoacoustic Imaging

Zhaoyong Li[1,*], Yanping Lin[1,*], Ting Qiu[2,*], Junsheng Liang[1], Yintao Lan[3], Fan Meng[4], Chaohao Liang[4], Yiqing Zhang[4], Qingyun Wang[1], Da Shi[1], Changli Zhang[1], Yanan Shi[1], Liujun Liu[1], Yanlan Yang[1], Jian Zhang[4,5]

[1]Department of Radiology, DongGuan Tungwah Hospital, Dongguan Key Laboratory of Radiology and Molecular Imaging, DongGuan, Guangdong, 523000, People's Republic of China; [2]Department of Radiology, Zhuhai People's Hospital (Zhuhai Hospital Affiliated with Jinan University), Zhuhai, Guangdong, 519000, People's Republic of China; [3]Guangzhou Regenerative Medicine and Health Guangdong Laboratory, Guangzhou, Guangdong, 510030, People's Republic of China; [4]School of Biomedical Engineering, Guangzhou Medical University, Guangzhou, Guangdong, 511436, People's Republic of China; [5]Department of Oncology, the Sixth Affiliated Hospital of Guangzhou Medical University, Qingyuan People's Hospital, Qingyuan, Guangdong, 511500, People's Republic of China

*These authors contributed equally to this work

Correspondence: Jian Zhang; Zhaoyong Li, Email jianzhang@gzhmu.edu.cn; lizhaoyong2003@163.com

Background: Photothermal therapy (PTT) guided by photoacoustic imaging (PAI) using nanoplatforms has emerged as a promising strategy for cancer treatment due to its efficiency and accuracy. This study aimed to develop and synthesize novel second near-infrared region (NIR-II) absorption-conjugated polymer acceptor acrylate-substituted thiadiazoloquinoxaline-diketopyrrolopyrrole polymers (PATQ-DPP) designed specifically as photothermal and imaging contrast agents for nasopharyngeal carcinoma (NPC).

Methods: The PATQ-DPP nanoparticles were synthesized and characterized for their optical properties, including low optical band gaps. Their potential as PTT agents and imaging contrast agents for NPC was evaluated both in vitro and in vivo. The accumulation of nanoparticles at tumor sites was assessed post-injection, and the efficacy of PTT under near-infrared laser irradiation was investigated in a mouse model of NPC.

Results: Experimental results indicated that the PATQ-DPP nanoparticles exhibited significant photoacoustic contrast enhancement and favorable PTT performance. Safety and non-toxicity evaluations confirmed the biocompatibility of these nanoparticles. In vivo studies showed that PATQ-DPP nanoparticles effectively accumulated at NPC tumor sites and demonstrated excellent tumor growth inhibition upon exposure to near-infrared laser irradiation. Notably, complete elimination of nasopharyngeal tumors was observed within 18 days following PTT.

Discussion: The findings suggest that PATQ-DPP nanoparticles are a promising theranostic agent for NIR-II PAI and PTT of tumors. This innovative approach utilizing PATQ-DPP nanoparticles provides a powerful tool for the early diagnosis and precise treatment of NPC, offering a new avenue in the management of this challenging malignancy.

Keywords: nasopharyngeal carcinoma, photoacoustic imaging, photothermal therapy, PATQ-DPP nanoparticles

Introduction

Currently, cancer remains a significant threat to public health globally and stands as one of the primary causes of death.[1,2] Notably, nasopharyngeal carcinoma (NPC) is recognized as one of the highly aggressive malignant tumors, occurring typically on the superior wall and lateral wall of the nasopharynx and displaying distinctive ethnic and regional distribution patterns.[3–5] The majority of new cases are reported in East and Southeast Asia,

Received: 28 December 2023
Accepted: 25 July 2024
Published: 31 July 2024

with China, in particular, being endemic to NPC.[6] In Southern China, NPC ranks as the third most prevalent cancer, with an incidence rate of 50 per 100,000.[7] What's worse, the morbidity and mortality of NPC have been upswing with the steady increase of EB virus infection rate in recent years.[8,9] However, conventional methodologies treatment, including surgical resection, chemotherapy, and radiotherapy, usually associated with many severe side effects and do not achieve complete cure.[10–12] Furthermore, traditional diagnostic methods such as magnetic resonance imaging, computerized tomography, and positron emission tomography have been proven effective in diagnosing NPC. However, these approaches come with numerous drawbacks and fall short of fulfilling the simultaneous requirements for minimal side effects, high resolution, and deep imaging depth.[13,14] Thus, it is imperative to explore imaging technologies and treatments to significantly improve efficacy and decrease complications.

Currently, with the rapid development of modern technology, precision medicine and targeted therapy have received interest from anticancer treatments.[15,16] Among the multifarious diagnosis and therapeutic methods, the combination of the photoacoustic imaging (PAI) and photothermal therapy (PTT) is one of the most powerful and noninvasive therapeutic tools which enables achieve the effect of remarkably therapeutic effects and few complications few side effects, high resolution and deep imaging depth simultaneously.[17–21] The fundamental principle of the PAI lies in the absorption of pulsed laser radiation energy by contrast agents in tissues. These agents subsequently convert this energy into an acoustic signal, which is then detected, measured, and visualized as an image through a scanning transducer.[22–24] Moreover, PAI stands out as an emerging nonionizing and non-invasive diagnostic technique that enables high-resolution and in-depth visualization of tissues.[25,26] The fundamental principle of the PTT involves a photothermal agent absorbing light and generating thermal energy to effectively ablate tumor cells.[27–33] PTT boasts several advantages, including non-invasiveness, high specificity, selectivity, and controllability.[34–36] Additionally, the utilization of the second near-infrared region (NIR-II) in the range of 1000–1700 nm for PTT offers improved tissue penetration depth (approximately 3–5 cm) and a higher maximum permissible exposure. Harnessing NIR-II light not only facilitates the treatment of deeper tumor regions but also allows for a robust power density, enhancing heat generation and thereby achieving high therapeutic efficacy in PTT.[37]

Commonly utilized contrast agents encompass metallic nanoparticles, carbon materials, and similar substances.[38–42] However, these materials are often plagued by degradability issues within tissues, posing a significant concern in clinical applications. Conjugated polymers have garnered increasing attention for diverse biomedical purposes, particularly in areas such as photodetectors, PTT, and PAI. Previous investigations primarily focused on homopolymers like poly-(3-hexylthiophene) and its derivatives as typical light-harvesting conjugated polymers. Nevertheless, these homopolymers exhibit substantial optical band gaps exceeding 2.0 eV, rendering them unable to absorb photons in the near-infrared (NIR) range.[43] Interestingly, in our previous research, we found that the PATQ-DPP nanoparticle is a low band gap polymer (0.56 eV).[44] The PATQ-DPP nanoparticles have a number of superior characteristics including good biocompatibility, high photoacoustic signal intensity and deep signal penetration. The PATQ-DPP nanoparticles was proven to be an efficient and stable contrast agents of in vivo photoacoustic and photothermal in the previous research.

As depicted in Figure 1, PATQ-DPP nanoparticles exhibited a specific accumulation in the tumor region attributed to retention effects and enhanced permeability. In the present study, we integrated PATQ-DPP nanoparticles with PTT and PAI in the NIR-II to investigate their therapeutic efficacy in nasopharyngeal carcinoma, a novel exploration in the field. A comprehensive set of characterizations and experiments were conducted, revealing uniform particle size, efficient thermal conversion, notable biocompatibility, and significant tumor ablation efficiency for the conjugated polymer PATQ-DPP nanoparticles, both in vivo and in vitro. In summary, the combination of NIR-II PAI-guided PTT using PATQ-DPP nanoparticles as therapeutic agents presents an efficient, promising and targeted treatment approach for the NPC.

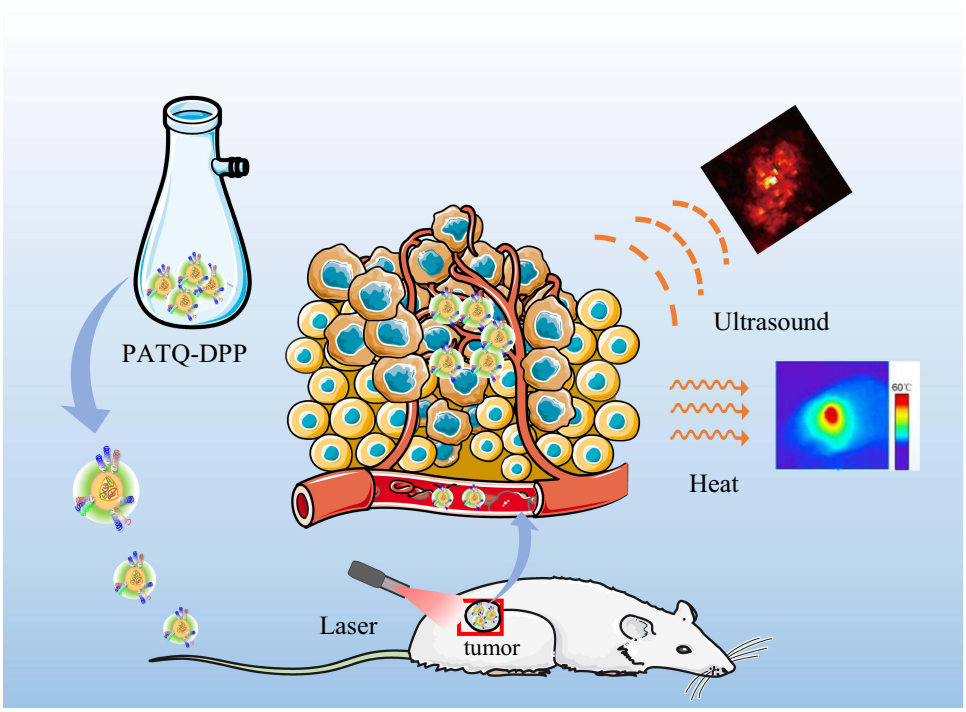

Figure 1 Schematic illustrations of PATQ-DPP nanoparticles for PAI guided PTT combination therapy of nasopharyngeal tumors.

Materials and Methods

Materials

Due to DongGuan Tungwah Hospital does not possess the necessary conditions for conducting animal research, and considering that this study requires such experiments, we utilized an animal facility (Guangdong Huamicro Testing Co., Ltd.) equipped with the appropriate qualifications. All animal experiments were conducted in accordance with the guidelines established by Institutional Animal Care and Use Committee and the Animal Care and Usage Committee of Guangdong Huawei Testing Co., Ltd. (FQ2021004-9). In this study, The BALB/c nude mice were procured from Zhuhai BesTest Bio-Tech Co., Ltd. The bovine serum albumin (BSA) was purchased from Shanghai Sigma Aldrich Biotechnology Co. Ltd. 3-(4,5-Dimethylthiazol-2-yl)-2,5-diphenyltetrazolium bromide (MTT) was obtained from Guangzhou Nice Biotechnology Co. Ltd. All other reagents and solvents were bought from commercial sources (Energy Chemical, Aldrich, and AVT Shanghai Pharmaceutical Tech, etc). And these materials were used without further purification. All the water used in the experiment was Ultrapure water (18.25 MΩ·cm, 25°C).

Synthesis and Preparation of Conjugated Polymers PATQ-DPP Nanoparticles

In this study, the material synthesis method in previous work published by our team has been adopted. The detailed methodology of this synthesis approach has been thoroughly documented in our earlier papers.[44] The synthesis protocol of PATQ-DPP nanoparticles[45,46] was performed as described below, the process is in Supplementary Figure 1. Briefly, four materials including M1 (71 mg, 64 μmol), M4 (76 mg, 64 μmol), Pd2(dba)3 (1.8 mg, 1.92 μmol) and P(o-tol)3 (2.5 mg, 7.7 μmol) were filled into a 5 mL dry reaction vial, and then they were undergone in it three vacuum-nitrogen cycles rapidly. Subsequently, 3 mL of freshly degassed chlorobenzene was introduced into the reaction vial. The resulting mixture underwent stirring and heating under a nitrogen atmosphere at 120°C for a duration of 12 hours. Afterward, the precipitate was obtained from the reaction mixture after it was cooled to room temperature and filtered using methanol. The polymer was further purified with acetone by Soxhlet and extracted with tetrahydro-furan by using Soxhlet apparatus. The precipitate was ultimately filtered and subjected to vacuum drying, resulting in the collection of dark blue PATQ-DPP (109 mg, 90%). After that, a THF solution (2 mL) containing DSPE-PEG 2000 (5.0 mg), conjugated

polymer (1.0 mg), chloro-form (1.0 mL) and ultra-purified water (10.0 mL) were mixed evenly and emulsified with sonication for 10 mins. Then the solution was concentrated under vacuum to evaporate the solvent. Next, the concentrated product was purified through a membrane filter (diameter = 220 nm). Finally, 1 mg/mL nanoparticle aqueous solution was obtained.

Characterization

The SHI-MADZU UV-2600 spectrophotometer (SHIMADZU, China) measured the optical absorption spectrum of the nanoparticles. The Malvern Nano-ZS Particle Sizer (Malvern, UK) carried out the Dynamic light scattering (DLS) characterization of the nanoparticles. JEOL's JEM-1400 Plus transmission microscope (JEOL, Japan) was utilized to obtain transmission electron microscopy (TEM) images of the nanoparticles. A homemade multispectral photoacoustic microscopy (MSPAM) system was utilized for the photoacoustic characterization.

Photothermal Property Test of the PATQ-DPP Nanoparticles in vitro

To evaluate the photothermal property of the PATQ-DPP nanoparticles, the nanoparticles' solution was initially diluted with PBS to four concentrations such as 0 μg/mL, 20 μg/mL, 40 μg/mL, and 80 μg/mL. Subsequently, 1 mL of each concentration was dispensed into a glass colorimetry cup and subjected to irradiation using a near-infrared laser with a wavelength of 980 nm for 10 mins. Two different power densities, namely 0.5 W/cm² and 1.0 W/cm², were applied. Finally, the temperature changes of the nanoparticles at various concentrations and power densities were monitored using an infrared thermal imaging camera (CEM, China).

Photoacoustic Performance of MSPAM System

In this investigation, we employed our MSPAM system to assess the photoacoustic properties of the PATQ-DPP nanoparticles. The schematic representation of the MSPAM system is illustrated in Supplementary Figure 2. The energy source for excitation comprised an ultrasound transducer with a central frequency of 25 MHz (Olympus, USA) and a wavelength-tunable nanosecond pulsed OPO laser (Continuum, USA). The obtained signals were subsequently amplified using an amplifier (Olympus, USA). The system was further comprised of a data acquisition module and a motorized 2D scanning stage. To evaluate the PAI capabilities of our MSPAM system, the imaging resolution and depth were rigorously tested and verified through a series of experiments. Additionally, the imaging resolution of our photoacoustic system was examined and confirmed. For depicting the resolution of our system, two strands of human hair (with a diameter less than 100 μm) were imaged. These hairs were embedded and stabilized in agar. In a maximum intensity projection (MIP) image featuring high contrast, the optical-absorption map of the agar-hair phantom was displayed in Supplementary Figure 3A. As demonstrated in Supplementary Figure 3B, the image profile along the dashed line was extracted from the MIP image. These experimental results underscored the system's capability to distinguish structures at the micrometer scale.

Cell Culture

In the experiment, human nasopharyngeal carcinoma cell lines CNE2 and Cos-7 were acquired from the American Type Culture Collection (ATCC). The CNE2 cell lines were cultivated in Roswell Park Memorial Institute-1640 (RPMI-1640) medium supplemented with 10% BSA and 1% penicillin-streptomycin (Gibco, USA). The Cos-7 cell lines were cultured in Dulbecco's Modified Eagle Medium (DMEM, Gibco) with 10% BSA and 1% penicillin/streptomycin (Corning). Both cell lines were maintained in the incubator at 37°C in 5% CO_2. Cells were utilized for assays and for constructing the nasopharyngeal carcinoma model once they reached the logarithmic growth phase.

In vitro Cytotoxicity Test of PATQ-DPP Nanoparticles

To assess the cytotoxicity of the obtained PATQ-DPP nanoparticles on COS-7 cells and CNE2 cells, an MTT assay was employed to estimate cell viability in vitro. During the logarithmic growth phase, Cos-7 cells and CNE2 cells ($1x10^4$ cells per well, 100 μL) were seeded in 96-well plates and cultured in a constant temperature incubator at 37°C with a 5% CO_2 concentration for 24 hours. Subsequently, the cells were exposed to PATQ-DPP nanoparticles aqueous solutions at

varying concentrations (0, 20, 40, 60, 80, 100 μg/mL) for an additional 24 hours. Following the incubation period, MTT solution (20 μL, 5000 μg/mL) was added to each well, and the 96-well plate was returned to the incubator for an additional 4 hours. Finally, an enzyme labeling apparatus was utilized to measure the absorbance (OD: 570 nm) of each well, allowing for the acquisition of experimental data on cell viability.

Animals and Tumor Model

Male BALB/c nude mice (5 weeks old) were selected to establish the NPC xenograft tumor model for in vivo experiments involving PAI and PTT. The CNE2 cells were cultured as described previously. The establishment of subcutaneous tumor models involved the injection of a CNE2 cell suspension (5×10^6 cells, 0.1 mL) into the right lateral side of BALB/c nude mice to induce tumor growth. When the tumor had reached a size of approximately 100 mm^3 (measured using the formula $V = ab^2/2$, where a and b represent the tumor's length and width, respectively), in vivo experiments were conducted.

In vivo PAI and PTT Experiments

To appraise the in vivo photoacoustic performance of PATQ-DPP nanoparticles in subcutaneous NPC tumors, initially, the NPC tumor-bearing nude mice were given an injection of a suspension of prepared nanoparticles (50 μL, 1 mg/mL). Subsequently, the mice were immediately put under anesthesia with sodium pentobarbital. The tumor location was imaged using our MSPAM system with 1064 nm laser excitation to obtain photoacoustic images at varying intervals over time (0, 6, 12, and 24 hours).

To evaluate the photothermal properties of PATQ-DPP nanoparticles in nude mice of nasopharyngeal tumors, 20 mice with a tumor volume of 100 mm^3 were chosen for in vivo PTT. We randomly divided the mice into four groups (n = 5 per group): (1) PATQ-DPP nanoparticles + Laser group, (2) PBS + Laser group, (3) PATQ-DPP nanoparticles + No laser group, and (4) Control group. Except for the control group and no laser PATQ-DPP nanoparticles group, all tumor-bearing nude mice were subjected to laser treatment under the same parameters (980 nm, 1 $W/cm,^2$ 10 mins). To investigate the therapeutic effect of the treatment, tumor volumes and body weights were measured in all mice every 3 days.

Histological Analysis

Firstly, immediately after the mice were sacrificed following the in vivo experiment, their vital organs, consisting of the heart, spleen, liver, lung, and kidneys, were harvested from each group. Then, the tissues were treated with a 4% paraformaldehyde solution for a period of 24 hours. Subsequently, tumor tissue slices were obtained through HE pathological staining experiments. Finally, tumor tissue samples were examined using an inverted light microscope to observe their pathological section results.

Results and Discussion

Synthesis and Characterization of the PATQ-DPP Nanoparticles

The conjugated polymer PATQ-DPP nanoparticles are considered a promising class of near-infrared polymers for applications in PAI and PTT.[47,48] In this study, the hydrodynamic diameter of the PATQ-DPP nanoparticles was obtained through the DLS. Figure 2A illustrates a hydrophilic diameter of approximately 70 nm. Subsequently, the morphology and size distribution of the PATQ-DPP nanoparticles were comprehensively characterized using TEM. As depicted in Figure 2B, TEM images revealed a predominantly regular spherical structure of PATQ-DPP nanoparticles, uniformly distributed in the solution, demonstrating favorable monodispersity. Moreover, the diameter observed through DLS closely matched that from TEM, suggesting precise and consistent measurements across different methods. Furthermore, the absorption spectra of PATQ-DPP nanoparticles were determined (Figure 2C), showing a strong and broad absorption spectrum spanning ranging from the visible to the near-infrared region. This broad absorption spectrum makes PATQ-DPP nanoparticles versatile and capable of meeting diverse requirements. The study indicated that PATQ-DPP nanoparticles exhibit strong NIR absorption, uniform morphology, and appropriate particle sizes.

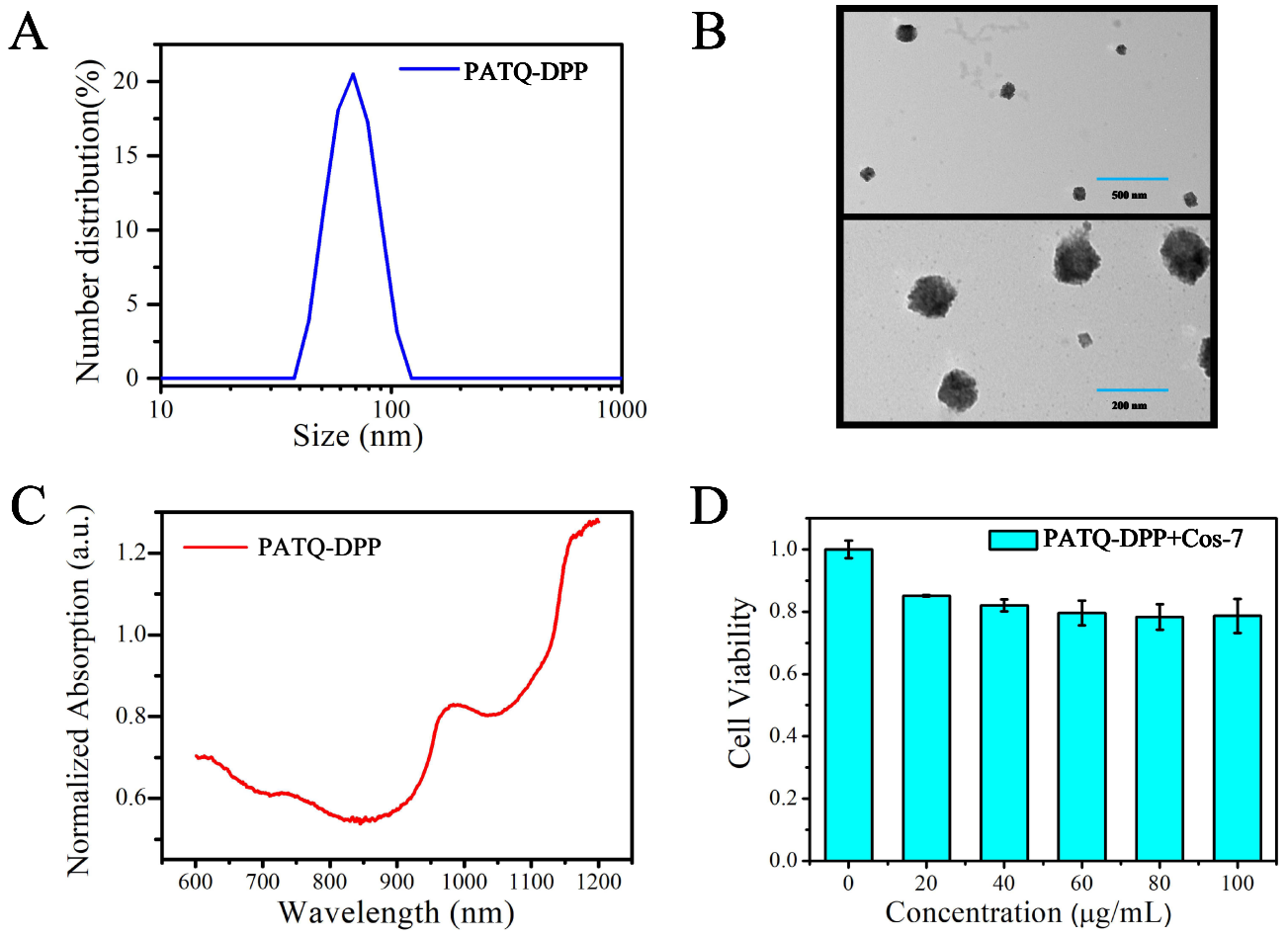

Figure 2 Characterizations and cytotoxicity of PATQ-DPP nanoparticles. (**A**) The DLS results of conjugated polymer PATQ-DPP nanoparticles in water. (**B**) TEM images of PATQ-DPP nanoparticles. (**C**) Absorbance spectrum change of PATQ-DPP nanoparticles. (**D**) Cell viabilities of Cos-7 cells incubated with the as prepared PATQ-DPP nanoparticles at different concentrations ranging from 0 μg/mL to 100 μg/mL.

Regarding the biocompatibility of PATQ-DPP nanoparticles, we have conducted a comprehensive evaluation in our preliminary research. A series of standard tests, including cytotoxicity assays, have been performed, and the results demonstrated that the material exhibits excellent biocompatibility under physiological conditions.[44] In this study, to re-evaluate the biocompatibility of PATQ-DPP nanoparticles in biomedical and clinical applications in vivo, their biocompatibility at the cellular level was assessed. Cytotoxicity of PATQ-DPP nanoparticles was evaluated using the MTT assay, as shown as in the Figure 2D and Supplementary Figure 5, illustrated that the viability of Cos-7 cells and CNE2 cells did not significantly differ with increasing concentrations of PATQ-DPP, highlighting the exceptional biocompatibility of these nanoparticles for biomedical and clinical use. In summary, the results demonstrated that PATQ-DPP nanoparticles possess suitable particle sizes, superior biostability, strong NIR absorption, and superior biocompatibility.

Photothermal Property of the PATQ-DPP Nanoparticles

In this study, various properties of the PATQ-DPP Nanoparticles have been validated by our previously published publications, particularly in terms of stability. The results indicated that even under extreme conditions, the material can maintain its structural and functional integrity.[44] Considering that the PATQ-DPP nanoparticles possess light absorption characteristics, this study used 980 nm diode laser to reveal the photothermal effect of PATQ-DPP nanoparticles. The thermographic images of PATQ-DPP nanoparticles solutions were achieved under the continuous laser irradiation for 10 mins with using infrared thermography, which were exhibited in Figure 3A. Quantitative monitoring of temperature changes was conducted across various concentrations (0, 20, 40, and 80 μg/mL) PATQ-DPP nanoparticles under 1.0 W/

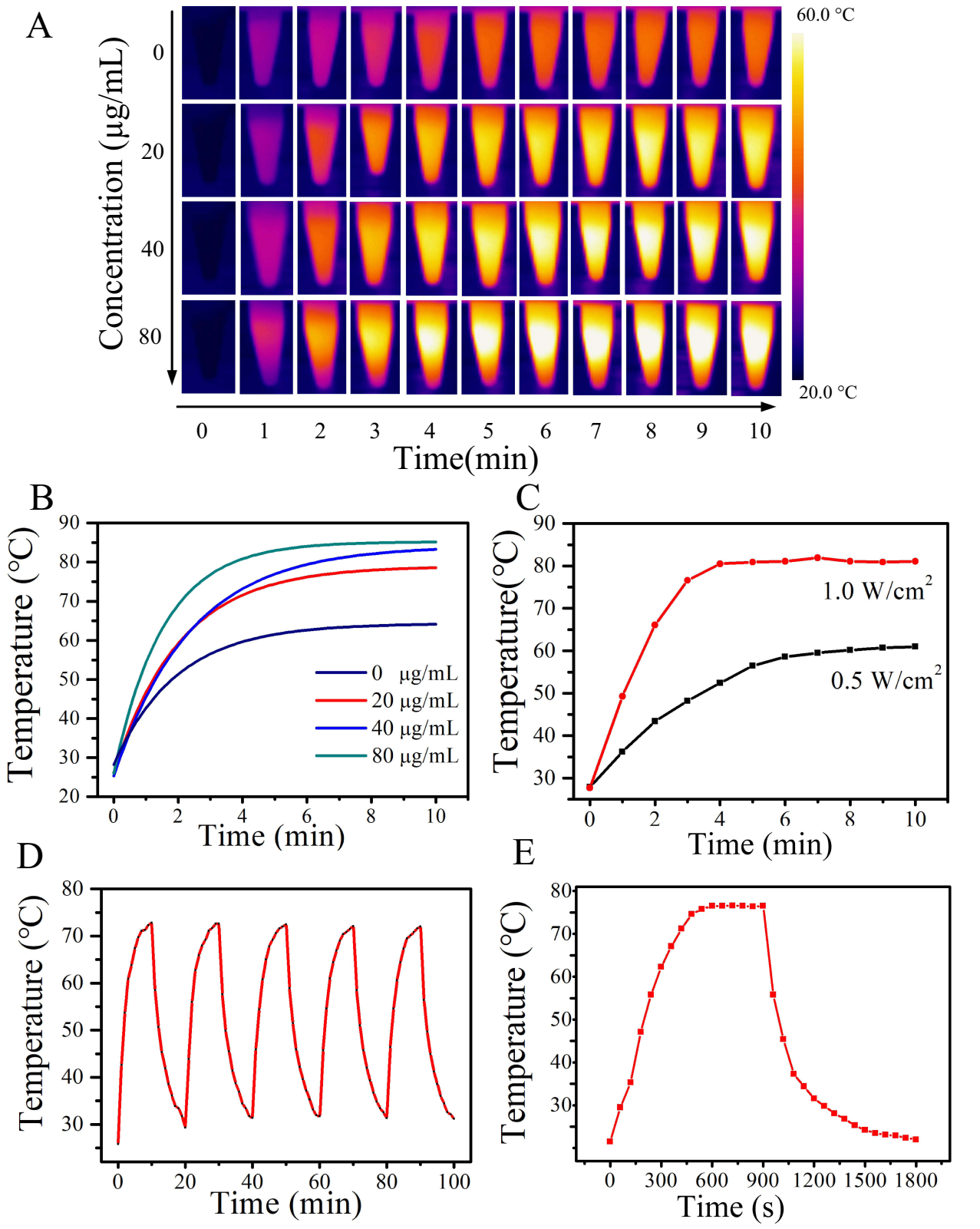

Figure 3 Photothermal ability of PATQ-DPP nanoparticles in vitro. (**A**) A series of photothermal images of the PATQ-DPP nanoparticles solution (0, 20, 40, 80 μg/mL) under NIR laser irradiation (1.0 W/cm^2, 980 nm). (**B**) The temperature variation of the solution containing different concentrations of the PATQ-DPP solution (0, 20, 40, 80 μg/mL) under the irradiation (1.0 W/cm^2, 980 nm). (**C**) Temperature elevation in the PATQ-DPP aqueous solution (1 mL, 80 μg/mL) under NIR laser exposure of 980 nm laser at different power densities. (**D**) Temperature variations of the PATQ-DPP nanoparticles under 980 nm laser irradiation at a power density of 1.0 W/cm^2 for five light on/off cycles laser irradiation. (**E**) The heating-cooling curves of the PATQ-DPP nanoparticles. Photothermal effect of PATQ-DPP (980 nm, 1 W/cm^2). The laser was switched off after irradiation for 10 mins.

cm^2 irradiation. The temperature increment of PATQ-DPP nanoparticles at a concentration of 80 μg/mL was particularly notable after 2 mins of illumination, reaching over 45°C (Figure 3B). The temperature increase of pure water was negligible, whereas the temperature of the PATQ-DPP solution increased rapidly with the prolonged laser irradiation time or increasing nanoparticle concentration, as demonstrated by infrared thermal images. These results demonstrated that PATQ-DPP nanoparticles efficiently converted absorbed photon energy into heat energy, showcasing potential for tumor cell destruction. Figure 3C visually illustrates that the temperature of the PATQ-DPP nanoparticle solution could reach 45°C even at a comparatively low laser power density (0.5 W/cm²), indicating effective tumor ablation. Moreover, nanoparticle stability is crucial for biological applications. Supplementary Figure 4 revealed no significant change in PATQ-DPP nanoparticles after 15 days of storage in different environments. Additionally, the photothermal stability of PATQ-DPP nanoparticles was evaluated through five laser on/off cycles under NIR laser irradiation (1 W/cm²). Surprisingly, after five cycles, the nanoparticles (80 μg/mL) maintained a consistent temperature level, indicating excellent photostability and reusability (Figure 3D). Furthermore, the study investigated the photothermal conversion efficiency (η) of PATQ-DPP nanoparticles,[44] a crucial parameter for assessing photothermal agents. The nanoparticles exhibited admirable stability and desirable photothermal conversion efficiency, which varied depending on factors such as power, concentration, and time, aligning with the concept of precision medicine to meet the diverse demands of patients with nasopharyngeal carcinoma at different phases (Figure 3E).

In vitro Photoacoustic Capability of the PATQ-DPP Nanoparticles

To validate the photoacoustic properties of PATQ-DPP nanoparticles, a series of experiments were conducted using the MSPAM system as previously introduced. Figure 4A illustrates that there was no substantial variation in photoacoustic signals over 50 mins under laser irradiation, indicating the good stability of enhanced photoacoustic (PA) imaging with PATQ-DPP nanoparticles. With the photostability of PATQ-DPP nanoparticles confirmed, the PAI was performed at varying concentrations (20, 40, 60, 80, and 100 μg/mL) using laser excitation at 980 nm. As shown in Figure 4B, even at low concentrations, PATQ-DPP nanoparticles still manifested a photoacoustic effect, and PA signals remarkably increased with higher nanoparticle concentrations. Figure 4C displays imaging profiles along the green dashed line

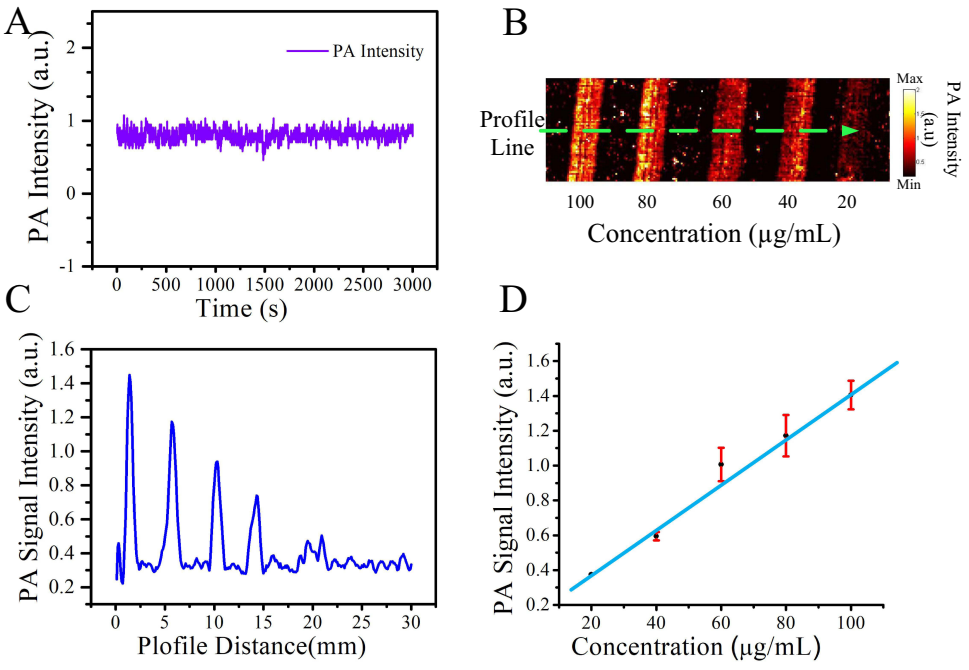

Figure 4 In vitro photoacoustic property of as-prepared PATQ-DPP nanoparticles. (**A**) The photostability of photoacoustic signal under the irradiation of different laser powers for 50 mins. (**B**) Photoacoustic images of PATQ-DPP nanoparticles under excitation at 980 nm at different concentrations. (**C**) Intensity profiles along the dashed line from (**B**). (**D**) The Photoacoustic amplitudes at 980 nm as a function of concentrations of PATQ-DPP nanoparticles.

from the photoacoustic image, revealing the sharp peaks signify the presence of PA signals at varying concentrations of nanoparticles. Importantly, the PA signal demonstrated a strong linear relationship with the concentration of PATQ-DPP nanoparticles, as shown in Figure 4D. In summary, these results indicated that PATQ-DPP nanoparticles exhibit admirable photoacoustic performance in vitro, showcasing their potential for use in PAI applications.

In vivo PAI of PATQ-DPP Nanoparticles

Base on the results above, the PAI capability of nanoparticles was attempted to be confirmed by using the nude mouse model. Brain blood vessels of the nude mouse model were conducted with our MSPAM system, and the results were recorded before and after injection PATQ-DPP nanoparticles. As shown in Figure 5A. the position and shape of a few brains blood vessels imaging were observed in a photoacoustic image before PATQ-DPP nanoparticles injection. After PATQ-DPP nanoparticles injection, the brain blood vessels performed clearer, which was shown in Figure 5B. These results indicated that the advantages of PAI with the aid of PATQ-DPP nanoparticles.

Surprised by the remarkable PAI performance as conducted above, in vivo PAI was attempted to be performed on the CNE2 tumor-bearing mice. When the tumor reaches a volume of approximately 100 mm^3, the CNE2 tumor-bearing mice were randomly divided into four groups of five mice per group. And then the PATQ-DPP suspensions (50 μL, 1 mg/mL) were injected into the mice. After injected the PATQ-DPP nanoparticles, the PA signals of tumor region at different times (0, 6, 12, 24 hours) were obtained by our MSPAM system. As revealed in Figure 5C, after 6 hours, a photoacoustic signal was observed and increased rapidly over time until 24 hours, which demonstrated that the PATQ-DPP nanoparticles had the ability of target CNE2 cells and could accumulate in the tumor site. Given the above, the results indicated that the PATQ-DPP

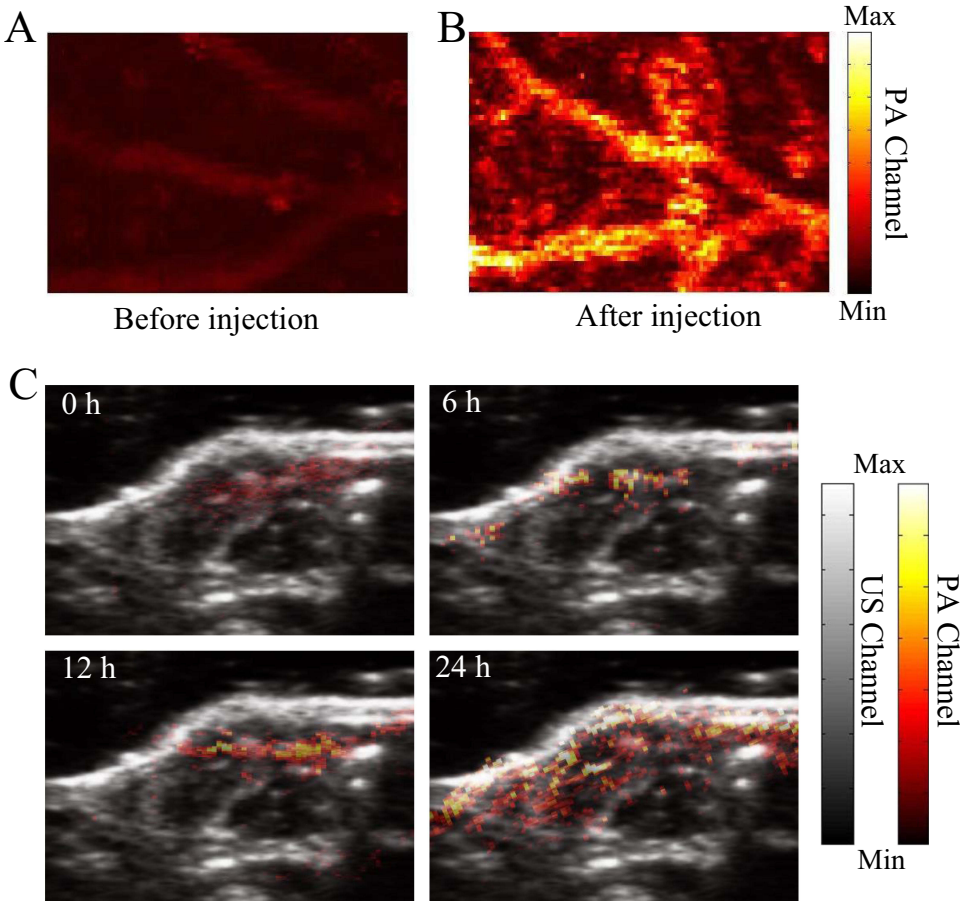

Figure 5 In vivo PAI of PATQ-DPP nanoparticles. Brain blood vessels images of the nude mouse model with our MSPAM system before (**A**) and after (**B**) the injection of PATQ-DPP nanoparticles. (**C**) Photoacoustic intensity in the tumor region after intravenously injection of PATQ-DPP nanoparticles at different time points.

nanoparticles possessed excellent tumor targeting accumulation in NPC tumor tissue, demonstrating exhilarating PAI effects and a long-lasting imaging period. In vivo multiscale PAI possesses the ability of comprehensive imaging of NPC.

In vivo PPT Based on PATQ-DPP Nanoparticles

Motivated by the efficient tumor accumulation of the nanoparticles, the curative effect of the NIR laser induced PTT of PATQ-DPP nanoparticles was evaluated in vivo with NPC tumor-bearing mice model, the exciting photoacoustic performance revealed the in vivo PTT capability of PATQ-DPP nanoparticles. NIR thermal imaging of PATQ-DPP nanoparticles in vivo was first explored under irradiation with 980 nm laser (1.0 W/cm^2) for 10 mins after orthotopic injection. This experiment was carried out on subcutaneous tumor-bearing nude mice, in which the tumor size reached approximately 100 mm^3. They were selected, then divided randomly into four groups (n = 5 per group) as follows, (1) PATQ-DPP nanoparticles + Laser group (1 W/cm^2, 10 mins), (2) PBS + Laser group (1 W/cm^2, 10 mins), (3) PATQ-DPP nanoparticles + No laser group, (4) Control group. As exhibited in Figure 6A, Hyperthermia was quickly generated in tumor region and raised to over 50 °C within 5 mins in the group treated with PATQ-DPP nanoparticles. While the results of the control group did not obvious change after 5 mins of laser irradiation, namely the temperature change was fully negligible. The results indicated that PATQ-DPP nanoparticles could serve as wonderful photothermal agents to generate hyperthermia in vivo to efficiently release hazardous substance and kill tumor cells.

Subsequently, to intuitively record long-term PTT efficacy and monitor the recovery process of PTT, the tumor volume of experimental mice and representative photographs were gathered and measured every 3 days after treatments. As revealed in Figure 6B, after laser hyperthermia treatment for 10 minutes, significantly dilated blood vessels were observed on the tumor surface in the NIR combined with PATQ-DPP nanoparticles-treated groups. The surface appeared slightly dark red, while other groups, after laser treatment for the same duration, showed less vasodilation on the surface, and the tumor appearance had no obvious change, with a slightly lighter color than the former. The results indicated that the growth rate of tumors in mice receiving single-factor treatment (only laser irradiation) was not significantly different from that of the control group without treatment and no laser PATQ-DPP nanoparticles-treated groups, indicating that laser irradiation alone and no laser PATQ-DPP nanoparticles-treated had no significant impact on tumor growth. At the previous treatment stage, the tumors treated by PATQ-DPP nanoparticles injection under laser irradiation displayed an admirable tumor ablation effect. Unexpectedly, complete tumor ablation with no recurrence was observed in 18 days by PATQ-DPP nanoparticles injection plus laser irradiation, while the tumors of other groups were growing rapidly, as marked with a green arrow in Figure 6B. These results confirmed that PATQ-DPP nanoparticles have excellent targeting treatment ability in vivo.

Furthermore, there were no substantial deviations in the body weight curves among the four groups, indicating that the treatments did not have a noticeable impact on the growth of the mice during the course of the experiment (Figure 6C). Meanwhile, it was observed that tumor volumes increased rapidly in the control groups throughout the experiment (Figure 6D). In summary, these results demonstrated that the combination of PATQ-DPP nanoparticles and PPT can serve as a promising and viable approach for cancer PTT in vivo with relatively minimal toxicity.

Histological Analysis

Furthermore, the mice were dissected after the in vivo experiment and the tumors were further studied using Hematoxylin and Eosin (H&E) staining. Each group of tumor tissue was subjected to H&E staining. As displayed in Figure 7A, the results showed that the PATQ-DPP nanoparticles plus laser irradiation group exhibited noticeable cell apoptosis and necrosis. In contrast, the groups with single-factor treatment (only laser irradiation) showed only partial destruction of tumor cells, while the tumor cells in the control group and the PATQ-DPP nanoparticles without laser group exhibited almost no necrotic tissue. These results demonstrated that PATQ-DPP nanoparticles have admirable photothermal properties and can effectively conduct chemo-PPT.

Last but not least, to further validate the biocompatibility of PATQ-DPP nanoparticles in vivo, mice were dissected after treatment, and major organs (heart, spleen, liver, lung, and kidneys) were examined using H&E staining. Compared with the control group, the results of the two groups were consistent, showing no obvious lesions and side effects in these major organs, was presented in Figure 7B. On the contrary, noticeable necrosis and cell apoptosis were observed in the

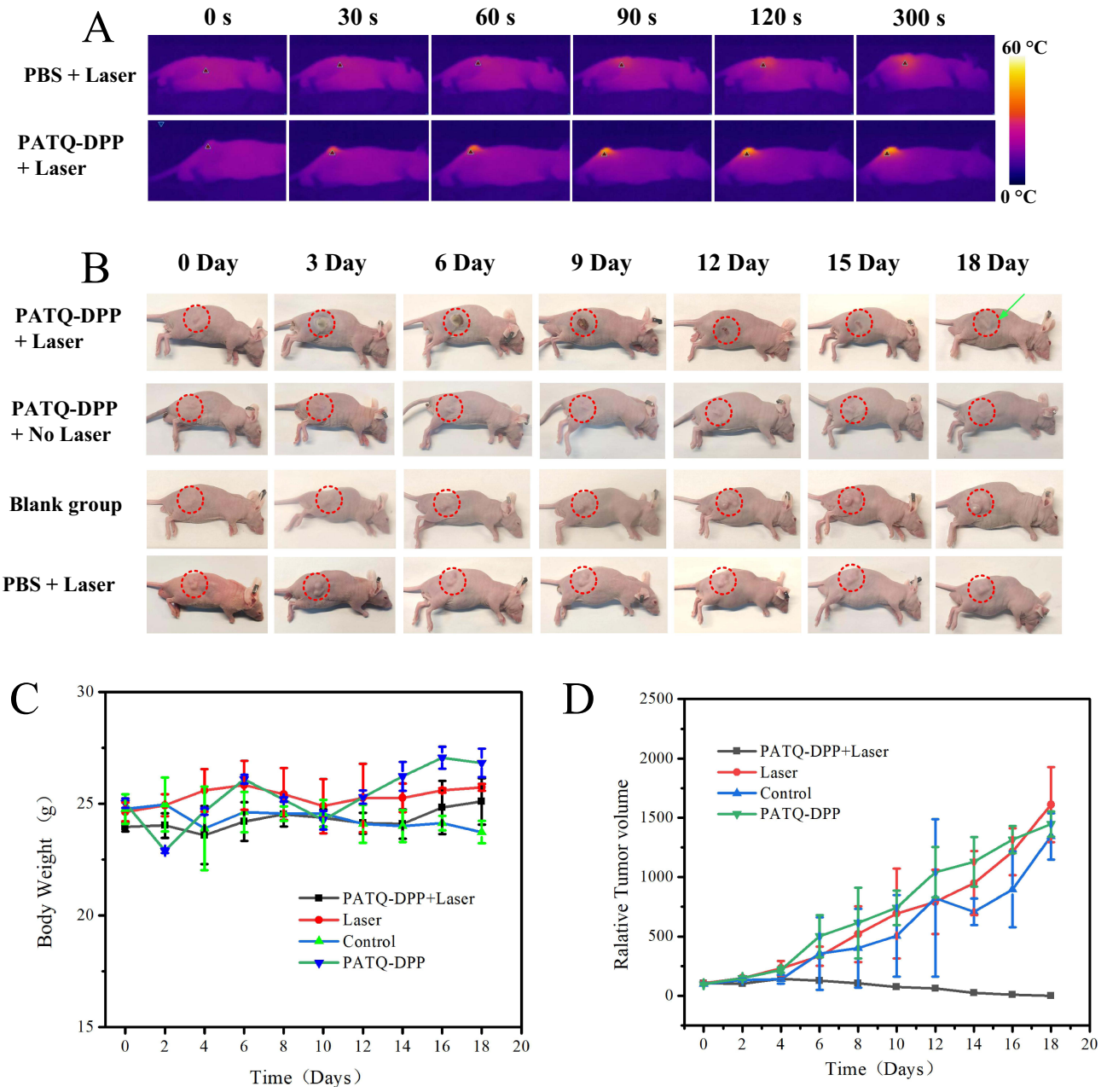

Figure 6 In vivo PTT of NPC tumor-bearing nude mice. (**A**) Photothermal images of NPC tumor-bearing mice injected with PBS and PATQ-DPP Nanoparticles (50 μL, 1 mg/ mL) under NIR laser irradiation (980 nm, 1 W/cm^2) for 5 mins at 6 h post-injection. (**B**) Representative photos of NPC tumor-bearing mice after different days before (0 day) and after (3, 6, 9, 12, 15 and 18 days) different treatments. (**C**) Average body weights of mice from each group after various treatments, and (**D**) Tumor volume changes of mice after different treatments: (1) The blue line represented Control group, no treatment. (2) The gray line represented PATQ-DPP Nanoparticles + Laser, injection of PATQ-DPP Nanoparticles with a laser. (3) The red line represented laser, irradiation with laser only. (4) The green line represented no laser, PATQ-DPP Nanoparticles only.

tumor after treatment with PATQ-DPP nanoparticles (Figure 7A), further indicating the insignificant cytotoxicity of PATQ-DPP nanoparticles to normal tissues while remarkably destroying the tumor tissues. In summary, the results presented substantiate that the obtained PATQ-DPP nanoparticles are an outstanding photothermal agent, with an eminent targeting accumulation ability toward nasopharyngeal carcinoma cells, consistent with the in vitro outcomes. Furthermore, these results suggested the security and low toxicity of PATQ-DPP nanoparticles, highlighting their potential as an effective platform for cancer PTT with relatively low systemic toxicity.

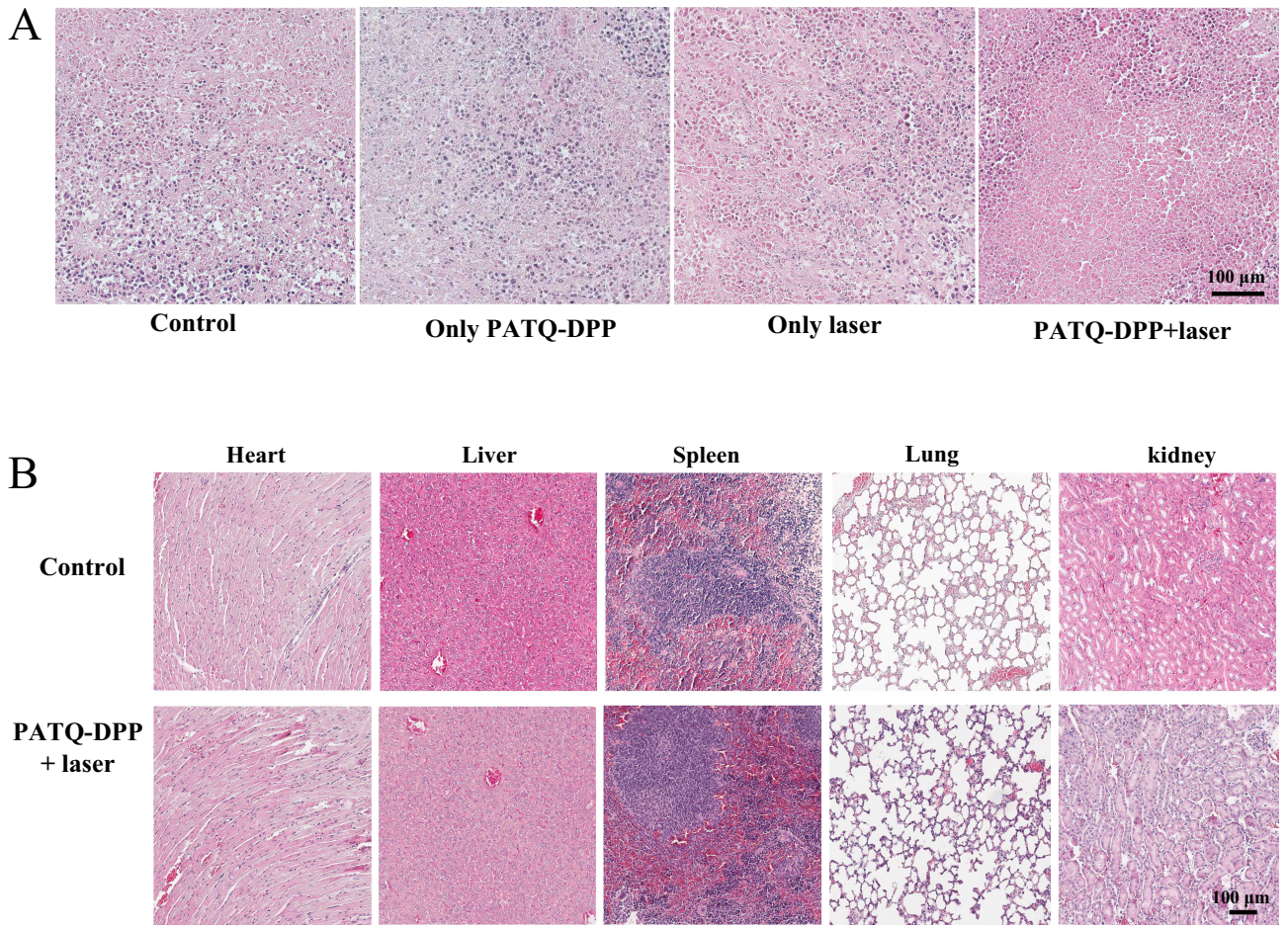

Figure 7 H&E staining of major organs and tumor from NPC tumor-bearing mice. (**A**) Histological section of tumor stained with hematoxylin and eosin. The scale bar is 100 μm. (**B**) Histological section of vital organs (heart, liver, spleen, lung and kidney) stained with hematoxylin and eosin after intravenous administration of PATQ-DPP nanoparticles. The scale bar is 100 μm.

Conclusion

In summary, we have resoundingly synthesized a novel low-band-gap conjugated polymer, PATQ-DPP nanoparticles, which good biocompatibility, prominent photothermal conversion, high photoacoustic signal intensity and deep signal penetration. Both in vitro and in vivo animal studies have shown that PATQ-DPP nanoparticles could simultaneously exhibit a photothermal effect under laser irradiation, enabling synergistic enhancement of PAI and PTT for the diagnosis and treatment of the NPC. The synthesized PATQ-DPP nanotheranostic platform exhibits significant potential for serving as a nanotheranostic tool for the precise diagnosis and treatment of NPC. It may surpass the limitations of conventional NPC treatments[49,50] and emerge as a novel strategy for NPC treatment. However, it's important to note that our current study was conducted using an NPC tumor-bearing mouse model with ectopic dorsal xenografts, which is limited by the experimental setup. Moving forward, we plan to upgrade our experimental equipment and delve deeper into the diagnosis and treatment of primary nasopharyngeal carcinoma through comprehensive research.

Acknowledgments

This research is supported by the Dongguan Science and Technology of Social Development Program (20231800940812) and the "520 Talent Plan" project of Tungwah Clinical Medical Research Institute of DongGuan (YJY202201), Guangzhou Science and Technology Plan Project (202102020140), and Guangdong Basic and Applied Basic Research Foundation (2020A1515011104).

Disclosure

The authors declare no conflicts of interest in this work.

References

1. Zhu L, Zhao J, Guo Z, et al. Applications of Aptamer-Bound Nanomaterials in Cancer Therapy. *Biosensors*. 2021;11(9):344. doi:10.3390/bios11090344
2. Chang M, Hou Z, Wang M. Recent advances in hyperthermia therapy-based synergistic immunotherapy. *Adv Mater*. 2021;33(4):2004788. doi:10.1002/adma.202004788
3. Zhu C, Jiang X, Xiao H. Tumor-derived extracellular vesicles inhibit HGF/c-Met and EGF/EGFR pathways to accelerate the radiosensitivity of nasopharyngeal carcinoma cells via microRNA-142-5p delivery. *Cell Death Discov*. 2022;8(1):1–11. doi:10.1038/s41420-021-00794-5
4. Pua LJW, Mai CW, Chung FF, et al. Functional roles of JNK and p38 MAPK signaling in nasopharyngeal carcinoma. *Int J Mol Sci*. 2022;23(3):1108. doi:10.3390/ijms23031108
5. Li W, Xu R, Zhu B, et al. Circular RNAs: functions and mechanisms in nasopharyngeal carcinoma. *Head Neck*. 2022;44(2):494–504. doi:10.1002/hed.26962
6. Wong KCW, Hui EP, Lo KW, et al. Nasopharyngeal carcinoma: an evolving paradigm. *Nat Rev Clin Oncol*. 2021;18(11):679–695. doi:10.1038/s41571-021-00524-x
7. Cao SM, Simons MJ, Qian CN. The prevalence and prevention of nasopharyngeal carcinoma in China. *Chin J Cancer*. 2011;30(2):114–119. doi:10.5732/cjc.010.10377
8. Tsang CM, Tsao SW. The role of Epstein-Barr virus infection in the pathogenesis of nasopharyngeal carcinoma. *Virol Sin*. 2015;30(2):107–121. doi:10.1007/s12250-015-3592-5
9. Yip YL, Lin W, Deng W. Establishment of a nasopharyngeal carcinoma cell line capable of undergoing lytic Epstein-Barr virus reactivation. *Lab Invest*. 2018;98(8):1093–1104. doi:10.1038/s41374-018-0034-7
10. Qiu T, Lan Y, Wei Z. In vivo multi-scale photoacoustic imaging guided photothermal therapy of cervical cancer based on customized laser system and targeted nanoparticles. *Int J Nanomed*. 2021;16:2879–2896. doi:10.2147/ijn.S301664
11. Liu Z, Chen Y, Su Y, et al. Nasopharyngeal Carcinoma: clinical Achievements and Considerations Among Treatment Options. *Front Oncol*. 2021;11:635737. doi:10.3389/fonc.2021.635737
12. Chen YP, Chan ATC, Le QT. Nasopharyngeal carcinoma. *Lancet*. 2019;394(10192):64–80. doi:10.1016/s0140-6736(19)30956-0
13. King AD. MR imaging of nasopharyngeal carcinoma. *Magn Reson Imaging C*. 2022;30(1):19–33. doi:10.1016/j.mric.2021.06.015
14. Yang SS, Wu YS, Chen WC. Benefit of [18F]-FDG PET/CT for treatment-naïve nasopharyngeal carcinoma. *Eur J Nucl Med Mol I*. 2022;49(3):980–991. doi:10.1007/s00259-021-05540-8
15. Shao J, Zaro J, Shen Y. Advances in exosome-based drug delivery and tumor targeting: from tissue distribution to intracellular fate. *Int J Nanomed*. 2020;15:9355–9371. doi:10.2147/IJN.S281890
16. Lin Y, Qiu T, Lan Y, et al. Multi-modal optical imaging and combined phototherapy of nasopharyngeal carcinoma based on a nanoplatform. *Int J Nanomed*. 2022;17:2435–2446. doi:10.2147/IJN.S357493
17. Zhong Y, Bejjanki NK, Miao X, et al. Synthesis and photothermal effects of intracellular aggregating nanodrugs targeting nasopharyngeal carcinoma. *Front Bioeng Biotechnol*. 2021;9:730925. doi:10.3389/fbioe.2021.730925
18. Riley RS, Day ES. Gold nanoparticle-mediated photothermal therapy: applications and opportunities for multimodal cancer treatment. *Wiley Interdiscip Rev Nanomed Nanobiotechnol*. 2017;9(4). doi:10.1002/wnan.1449
19. Sun J, Cai W, Sun Y, et al. Facile synthesis of melanin-dye nanoagent for NIR-II fluorescence/photoacoustic imaging-guided photothermal therapy. *Int J Nanomed*. 2020;15:10199–10213. doi:10.2147/IJN.S284520
20. Ding H, Cai Y, Gao L. Exosome-like nanozyme vesicles for H2O2-responsive catalytic photoacoustic imaging of xenograft nasopharyngeal carcinoma. *Nano Lett*. 2018;19(1):203–209. doi:10.1021/acs.nanolett.8b03709
21. Gröhl J, Schellenberg M, Dreher K, Maier-Hein L. Deep learning for biomedical photoacoustic imaging: a review. *Photoacoustics*. 2021;22:100241. doi:10.1016/j.pacs.2021.100241
22. Beard P. Biomedical photoacoustic imaging. *Interface Focus*. 2011;1(4):602–631. doi:10.1098/rsfs.2011.0028
23. Lei S, Zhang J, Blum NT. In vivo three-dimensional multispectral photoacoustic imaging of dual enzyme-driven cyclic cascade reaction for tumor catalytic therapy. *Nat Commun*. 2022;13(1):1–14. doi:10.1038/s41467-022-29082-1
24. Zharov VP. Ultrasharp nonlinear photothermal and photoacoustic resonances and holes beyond the spectral limit. *Nat Photonics*. 2011;5(2):110–116. doi:10.1038/nphoton.2010.280
25. Liu Y, Nie L, Chen X. Photoacoustic molecular imaging: from multiscale biomedical applications towards early-stage theranostics. *Trends Biotechnol*. 2016;34(5):420–433. doi:10.1016/j.tibtech.2016.02.001
26. Lyu Y, Zeng J, Jiang Y. Enhancing both biodegradability and efficacy of semiconducting polymer nanoparticles for photoacoustic imaging and photothermal therapy. *ACS Nano*. 2018;12(2):1801–1810. doi:10.1021/acsnano
27. Li X, Lovell JF, Yoon J. Clinical development and potential of photothermal and photodynamic therapies for cancer. *Nat Rev Clin Oncol*. 2020;17(11):657–674. doi:10.1038/s41571-020-0410-2
28. Kharlamov AN, Zubarev IV, Shishkina EV. Nanoparticles for treatment of atherosclerosis: challenges of plasmonic photothermal therapy in translational studies. *Future Cardiol*. 2018;14(2):109–114. doi:10.2217/fca-2017-0051
29. Pei P, Yang F, Liu J. Composite-dissolving microneedle patches for chemotherapy and photothermal therapy in superficial tumor treatment. *Biomater Sci*. 2018;6(6):1414–1423. doi:10.1039/c8bm00005k
30. Jaque D, Maestro LM, Rosal B. Nanoparticles for photothermal therapies. *Nanoscale*. 2014;6(16):9494–9530. doi:10.1039/c4nr00708e
31. Liu Q, Liu L, Mo C. Polyethylene glycol-coated ultrasmall superparamagnetic iron oxide nanoparticles-coupled sialyl Lewis X nanotheranostic platform for nasopharyngeal carcinoma imaging and photothermal therapy. *J Nanobiotechnol*. 2021;19(1):1–14. doi:10.1186/s12951-021-00918-0
32. Huang X, Jain PK, El-Sayed IH. Plasmonic photothermal therapy (PPTT) using gold nanoparticles. *Laser Med Sci*. 2008;23(3):217–228. doi:10.1007/s10103-007-0470-x

33. Wang M. Emerging multifunctional NIR photothermal therapy systems based on polypyrrole nanoparticles. *Polymers*. 2016;8(10):373. doi:10.3390/polym8100373
34. Zou L, Wang H, He B, et al. Current approaches of photothermal therapy in treating cancer metastasis with nanotherapeutics. *Theranostics*. 2016;6(6):762–772. doi:10.7150/thno.14988
35. Shen S, Wang S, Zheng R, et al. Magnetic nanoparticle clusters for photothermal therapy with near-infrared irradiation. *Biomaterials*. 2015;39:67–74. doi:10.1016/j.biomaterials.2014.10.064
36. Wang F, Zhu J, Wang Y. Recent advances in engineering nanomedicines for second near-infrared photothermal-combinational immunotherapy. *Nanomaterials*. 2022;12(10):1656. doi:10.3390/nano12101656
37. Fu Q, Zhu R, Song J. Photoacoustic imaging: contrast agents and their biomedical applications. *Adv Mater*. 2019;31(6):1805875. doi:10.1002/adma.201805875
38. Wu D, Huang L, Jiang MS. Contrast agents for photoacoustic and thermoacoustic imaging: a review. *Int J Mol Sci*. 2014;15(12):23616–23639. doi:10.3390/ijms151223616
39. Gong H, Peng R, Liu Z. Carbon nanotubes for biomedical imaging: the recent advances. *Adv Drug Deliv Rev*. 2013;65(15):1951–1963. doi:10.1016/j.addr.2013.10.002
40. Wang S, Lin J, Wang T. Recent advances in photoacoustic imaging for deep-tissue biomedical applications. *Theranostics*. 2016;6(13):2394–2413. doi:10.7150/thno.16715
41. Hahn MA, Singh AK, Sharma P. Nanoparticles as contrast agents for in-vivo bioimaging: current status and future perspectives. *Anal Bioanal Chem*. 2011;399(1):3–27. doi:10.1007/s00216-010-4207-5
42. Pu K, Shuhendler AJ, Jokerst JV, et al. Semiconducting polymer nanoparticles as photoacoustic molecular imaging probes in living mice. *Nat Nanotechnol*. 2014;9(3):233–239. doi:10.1038/nnano.2013.302
43. Thompson BC, Frechet JM. Polymer-fullerene composite solar cells. *Angew Chem Int Ed Engl*. 2008;47:58–77. doi:10.1002/anie.200702506
44. Luo Y, Lan Y, Peng L. Acrylate-substituted thiadiazoloquinoxaline yields ultralow band gap (0.56 eV) conjugated polymers for efficient photoacoustic imaging. *ACS Appl Polym Mater*. 2021;3(6):3247–3253. doi:10.1021/ACSAPM.1C00464
45. Cao Z, Chen J, Liu S, et al. Understanding of imine substitution in wide-bandgap polymer donor-induced efficiency enhancement in all-polymer solar cells. *Chem Mater*. 2019;31:8533–8542. doi:10.1021/acs.chemmater.9b03570
46. Zhao J, Li Q, Liu S, et al. Bithieno [3,4-c]pyrrole-4,6-dione-mediated crystallinity in large bandgap polymer donors directs charge transportation and recombination in efficient nonfullerene polymer solar cells. *ACS Energy Lett*. 2020;5(2):367–375. doi:10.1021/acsenergylett.9b02842
47. Wang Y, Feng L, Wang S. Conjugated polymer nanoparticles for imaging, cell activity regulation, and therapy. *Adv Funct Mater*. 2019;29:1806818. doi:10.1002/adfm.201806818
48. Smith AM, Mancini MC, Nie S. Bioimaging: second window for in vivo imaging. *Nat Nanotechnol*. 2009;4(11):710–711. doi:10.1038/nnano.2009.326
49. Hua YJ, Han F, Lu LX, et al. Long-term treatment outcome of recurrent nasopharyngeal carcinoma treated with salvage intensity modulated radiotherapy. *Eur J Cancer*. 2012;48(18):3422–3428. doi:10.1016/j.ejca.2012.06.016
50. Huang H, Yao Y, Deng X, et al. Immunotherapy for nasopharyngeal carcinoma: current status and prospects. *Int J Oncol*. 2023;63(2):97. doi:10.3892/ijo.2023.5545